JBC Papers in Press. Published on May 22, 2009 as Manuscript M109.010264
The latest version is at http://www.jbc.org/cgi/doi/10.1074/jbc.M109.010264

TDP-43 IS INTRINSICALLY AGGREGATION-PRONE AND ALS-LINKED MUTATIONS ACCELERATE AGGREGATION AND INCREASE TOXICITY

Brian S. Johnson[1], David Snead[2], Jonathan J. Lee[1], J. Michael McCaffery[3], James Shorter[2], Aaron D. Gitler[1]

From Department of Cell and Developmental Biology[1] and Department of Biochemistry and Biophysics[2], The University of Pennsylvania School of Medicine, Philadelphia PA 19104 and Integrated Imaging Center and Department of Biology[3], Johns Hopkins University, Baltimore MD, 21218

Running head: ALS mutations accelerate TDP-43 aggregation

Address correspondence to: Aaron D. Gitler, 1109 BRB II/III, 421 Curie Blvd., Philadelphia, PA 19104. Phone: 215-573-8251; Fax: 215-898-9871; E-mail: gitler@mail.med.upenn.edu or James Shorter, 805B Stellar-Chance Laboratories, 422 Curie Blvd., Philadelphia, PA 19104. Phone: 215-573-4256; Fax: 215-898-9871; E-mail: jshorter@mail.med.upenn.edu

Non-amyloid, ubiquitinated cytoplasmic inclusions containing TDP-43 and its C-terminal fragments are pathological hallmarks of amyotrophic lateral sclerosis (ALS), a fatal motor neuron disorder, and frontotemporal lobar degeneration with ubiquitin-positive inclusions (FTLD-U). Importantly, TDP-43 mutations are linked to sporadic and non-SOD1 familial ALS. However, TDP-43 is not the only protein in disease-associated inclusions and whether TDP-43 misfolds or is merely sequestered by other aggregated components is unclear. Here, we report that in the absence of other components, TDP-43 spontaneously forms aggregates bearing remarkable ultrastructural similarities to TDP-43 deposits in degenerating neurons of ALS and FTLD-U patients. The C-terminal domain of TDP-43 is critical for spontaneous aggregation. Several ALS-linked TDP-43 mutations within this domain (Q331K, M337V, Q343R, N345K, R361S, and N390D) increase the number of TDP-43 aggregates and promote toxicity *in vivo*. Importantly, mutations that promote toxicity *in vivo* accelerate aggregation of pure TDP-43 *in vitro*. Thus, TDP-43 is intrinsically aggregation-prone and its propensity for toxic misfolding trajectories is accentuated by specific ALS-linked mutations.

TDP-43 is a ubiquitously expressed and highly conserved metazoan nuclear protein (1), which contains two RNA recognition motifs (RRMs) and a glycine-rich region in its C-terminal domain (Fig. 1A). TDP-43 function is uncertain, but it likely plays important roles in pre-mRNA splicing and transcriptional repression (2,3). In ALS and FTLD-U, TDP-43 is depleted from the nucleus and accumulates in ubiquitinated cytoplasmic inclusions (4). These, and other situations of TDP-43 pathology, including some forms of Alzheimer's and Parkinson's diseases, are now known as TDP-43 proteinopathies (5). Importantly, mutations in the TDP-43 gene (*TARDBP*) are linked to sporadic and non-SOD1 familial ALS, implying that TDP-43 abnormalities are likely one cause of disease (6-11). However, despite this synthesis of pathology and genetics, the mechanisms by which TDP-43 might contribute to disease remain unknown and controversial (12,13).

A key unresolved question is whether TDP-43 is inherently aggregation-prone or whether TDP-43 is sequestered by other aggregated components and is merely a marker of disease (13-16). Indeed, multiple proteins aside from TDP-43 are found in sarkosyl insoluble fractions from FTLD-U patients (14). Moreover, deconvolution imaging reveals that TDP-43 appears to be excluded from some regions of the ubiquitinated inclusions in ALS (15).

Here, we assess TDP-43 aggregation in the absence of other components. We then define which domains of TDP-43 are important

for this process and determine the direct effects of several ALS-linked TDP-43 mutations on TDP-43 misfolding and toxicity. Our findings bring to light several intrinsic properties of TDP-43 and ALS-linked TDP-43 mutants that likely play important roles in the aberrant TDP-43 proteostasis (17) that contributes to the pathogenesis of ALS, FTLD-U and other TDP-43 proteinopathies.

Experimental Procedures

Yeast Strains, Media, and Plasmids

Yeast cells were grown in rich media (YPD) or in synthetic media lacking uracil and containing 2% glucose (SD/-Ura), raffinose (SRaf/-Ura), or galactose (SGal/-Ura).

A TDP-43 Gateway¨ entry clone was obtained from Invitrogen, containing full-length human TDP-43 in the vector pDONR221. To generate C-terminally YFP-tagged TDP-43 constructs, we used PCR to amplify TDP-43 without a stop codon and incorporate Spe I and Hind III restriction sites along with a Kozak consensus sequence. The resulting PCR product was cloned into Spe I / Hind III digested pRS416GAL-YFP) to generate the CEN TDP-43YFP fusion construct. Each ALS-linked TDP-43 mutant construct was generated by using the QuikChange® site-directed mutagenesis system (Stratagene) with pRS416GAL-TDP-43-YFP as template. All constructs were verified by DNA sequencing. CEN plasmid constructs (e.g. pRS416GAL-TDP-43-YFP) were transformed into BY4741 (*MATa his3 leu2 met15 ura3*).

Yeast transformation and spotting assays

Yeast procedures were performed according to standard protocols. We used the PEG/lithium acetate method to transform yeast with plasmid DNA. For spotting assays, yeast cells were grown overnight at 30°C in liquid media containing SRaf/-Ura until they reached log or mid-long phase. Cultures were then normalized for OD_{600nm}, serially diluted and spotted with a Frogger (V&P Scientific) onto synthetic solid media containing glucose (SD/-Ura) or galactose (SGal/-Ura) lacking uracil and were grown at 30°C for 2-3 days.

Yeast survivorship assay

We performed survivorship assays as described previously (18). Briefly, after induction of empty vector, wild type (WT) or mutant TDP-43 in 2% galactose, survivorship was determined at the indicated time-points by harvesting cells at an OD_{600nm} of 1, diluting them 1:1000 and plating 300 µl of these cells on synthetic media containing 2% glucose (represses TDP-43 expression). Plates were incubated at 30°C for 2 days. Colony forming units were then determined.

Immunoblotting

Yeast lysates were subjected to SDS/PAGE (4-12% gradient, Invitrogen) and transferred to a PVDF membrane (Invitrogen). Membranes were blocked with 5% nonfat dry milk in PBS for 1 hr at room temperature or overnight at 4°C. Primary antibody incubations were performed at room temperature for 1 hour. After washing with PBS, membranes were incubated with a horseradish peroxidase-conjugated secondary antibody for 1 hr at room temperature, followed by washing in PBS+0.1% Tween 20 (PBST). Proteins were detected with Immobilon Western HRP Chemiluminescent Substrate (Millipore). The anti-GFP monoclonal antibody (Roche) was used at 1:10,000, Phosphoglycerate Kinase 1 (Pgk1) antibody (Invitrogen) at 1:500. The HRP-conjugated anti-mouse secondary antibody was used at 1:5000.

Immunocytochemistry

For immunocytochemistry experiments, yeast cells expressing untagged TDP-43 constructs were grown to a final OD600 of 0.2-0.8 and then fixed with 3.7% formaldehyde for 1 h. Cells were collected by centrifugation at 2000rpm for 5 min and washed in PBS. The cells were diluted and washed once before resuspending in 1mL of Solution A (0.5mM $MgCl_2$, 1.2M Sorbitol, 40mM K_3PO_4 pH 6.5). Cells were incubated with 10µl of 2-mercaptoethanol and 25µl of 10mg/mL lyticase for 15 min at 37°C. Spheroplasted cells were collected at 4000rpm for 5 min, washed twice with Solution A and once with PBS, and resuspended in PBS+BSA (1X PBS, 1mg/mL bovine serum albumin). Spheroplasts were diluted 1:5, and incubated on Teflon-covered slides treated with 1mg/ml poly-lysine. Wells were blocked with PBS+BSA for 30 min at room temperature. Primary antibody incubations using 1:200 anti-TDP-43 mouse polyclonal antibody

(Novus) were performed for 1.5 h at room temperature. After washing with PBS-BSA, wells were incubated with 1:2000 Alexa 488nm donkey anti-mouse polyclonal antibody (Invitrogen) for 1.5 h at room temperature. After washing with PBS-BSA, wells were incubated with Vectashield mounting medium containing 1.5μg/mL DAPI (Vector Labs) for 5 min before visualization using fluorescence microscopy.

Sedimentation analysis

We performed sedimentation analysis as described in (19). Cells expressing either YFP-tagged TDP-43 constructs or CFP-tagged polyglutamine-expanded huntingtin constructs for 4 or 6h were lysed in 1x native yeast lysis buffer (30mM HEPES pH 8.0, 150mM NaCl, 1% glycerol, 1mM DTT, 0.5% Triton X-100, 1mM PMSF, 50mM NEM, 1X protease inhibitor cocktail (Roche)). Cells were disrupted in a bead beater for 3 min at 4°C. Cellular debris was removed by centrifugation at 6,000 x g for 5 min at 4°C. The yeast lysate was separated into a total fraction and a pellet fraction. After the pellet fraction was spun at either 16,000 x g or 85,000 rpm in a TLA 100.1 rotor for 30 min at 4°C the supernatant was recovered and designated the soluble fraction. The pellet fraction was resolubilized by boiling in 50μl 1X SDS sample buffer. The total and soluble fractions were boiled in equal volumes of 4X SDS sample buffer. 20% of the pellet fraction and 10% of soluble and total fractions were resolved by SDS-PAGE followed by immunoblotting with anti-GFP antibody.

Fluorescence Microscopy

For fluorescence microscopy experiments, single colony isolates of the yeast strains were grown to mid-log phase in SRaf/-Ura media at 30°C. Cultures were spun down and resuspended in the same volume of SGal/-Ura to induce expression of the TDP-43-YFP constructs. Cultures were induced with galactose for 6h before being fixed with 70% ethanol and stained with DAPI in Vectashield mounting medium (Vector Labs) to visualize nuclei. Images were obtained using a Zeiss Axioplan Upright Microscope and a Zeiss AxioCam HRm high-resolution monochrome CCD camera. The images were deblurred using a nearest neighbor algorithm in the AxioVision 4.5 software and representative cells were chosen for figures.

Quantification of TDP-43 Aggregation

To assess differences in aggregation between wild-type and mutant TDP-43, yeast cultures were grown, induced and processed as described above after having normalized all yeast cultures to OD_{600nm}=0.2 prior to galactose induction. After 6h of induction, the identities of the samples were blinded to the observer before being examined. Several fields of cells were randomly chosen using the DAPI filter to prevent any bias towards populations of cells with increased amounts of aggregation in addition to obtaining the total number of cells in any given field. At least 200 cells per sample were counted for each replicate. Only cells with greater than 3 foci under the YFP channel were considered as cells with aggregating TDP-43.

TDP-43 purification

TDP-43 and various missense (G294A, M337V or Q331K) or deletion mutants (1-275 or 188-414) were expressed and purified from *E. coli* as either his-tagged or GST-tagged proteins. For his-tagged preparations, TDP-43 was cloned into pCOLD I (Takara) and overexpressed in *E. coli* BL21 (RIL). Cells were lysed by sonication on ice in 40mM Hepes-KOH pH 7.4, 500mM KCl, 20mM $MgCl_2$, 10% glycerol, 20mM imidazole, 2mM βmercaptoethanol, and protease inhibitors (complete, EDTA-free, Roche). The proteins were purified over a Ni-NTA column (Qiagen). For GST-tagged preparations, TDP-43 was cloned into GV13 to yield GST-TEV-TDP-43, and overexpressed in *E. coli* BL21 (DE3) RIL or Rosetta2 (Novagen). Protein was purified over a glutathione-sepharose column (GE) according to manufacturer's instructions. GST was then removed by cleavage with TEV protease (Invitrogen), and protease and GST were removed using Ni-NTA and glutathione-sepharose. His-tagged and untagged TDP-43 proteins were ~95% pure as assessed by SDS-PAGE. His-tagged and untagged proteins aggregated with identical kinetics and formed aggregates with very similar morphologies.

After purification, proteins were buffer exchanged into assembly buffer (AB): 40mM HEPES-KOH pH 7.4, 150mM KCl, 20mM $MgCl_2$, 1mM DTT. Proteins were filtered

through a 0.22μm filter. After filtration, the protein concentration was determined by Bradford assay (Bio-Rad) and the proteins were used immediately for aggregation reactions.

For size exclusion chromatography, Superdex-200 10/300 GL analytical gel filtration column (GE) was calibrated with thyroglobulin (669kDa), ferritin (440kDa), bovine serum albumin (67kDa), β-lactoglobulin (35kDa), ribonuclease A (13.7kDa), and aprotinin (6.5kD). TDP-43 was incubated in AB at 25°C with agitation for 5min and any insoluble material was removed by centrifugation at 16,100g for 5min. Protein was loaded onto the calibrated Superdex-200 10/300 GL column equilibrated in AB, and eluted at 0.4ml/min. Oligomeric fractions were pooled and processed for electron microscopy (see below).

TDP-43 aggregation in vitro

Filtered, purified TDP-43 was used immediately for aggregation assays. TDP-43 or missense mutant TDP-43 or deletion mutants (3μM) were incubated at 25°C in AB for 0-120min with agitation at 1400rpm in an Eppendorf Thermomixer. Turbidity was used to assess aggregation by measuring absorbance at 395nm. For sedimentation analysis, reactions were centrifuged at 16,100g for 30min at 25°C. Supernatant and pellet fractions were then resolved by SDS-PAGE and stained with Coomassie Brilliant Blue, and the amount in either fraction determined by densitometry in comparison to known quantities of TDP-43. Alternatively, reactions were processed for Congo Red binding or Thioflavin-T fluorescence as described (20).

For electron microscopy (EM) of in vitro aggregation reactions, TDP-43 protein samples (10μl of a 3μM solution) were adsorbed onto glow-discharged 300 mesh formvar/carbon-coated copper grid (Electron Microscopy Sciences) and stained with 2% (w/v) aqueous uranyl acetate. Excess liquid was removed and grids were allowed to air dry. Samples were viewed using a JEOL 1010 transmission electron microscope. Images were captured with a Hamamatsu digital camera using AMT acquisition software.

Electron microscopy of yeast cells

Conventional EM was performed as previously described (21). Briefly, the cells were fixed in 3% glutaraldehyde contained in 0.1M Na cacodylate, pH 7.4, 5mM $CaCl_2$, 5mM $MgCl_2$, and 2.5% sucrose for 1 hour at 25°C with gentle agitation; spheroplasted; embedded in 2% ultra low temperature agarose (prepared in water); cooled; and subsequently cut into small pieces (~1mm^3). The cells are then post-fixed in 1% OsO_4/ 1% potassium ferrocyanide contained in 0.1M cacodylate/ 5mM $CaCl_2$, pH 7.4 for 30 minutes at room temperature. The blocks are washed thoroughly 4X with ddH_20, 10 minutes total; transferred to 1% thiocarbohydrazide at room temperature for 3 minutes; washed in ddH_2O (4X, 1 minutes each); and transferred to 1% OsO_4/ 1% potassium ferrocyanide in cacodylate buffer pH 7.4 for an additional 3 minutes at room temperature. The cells are then washed 4X with ddH_2O (15 minutes total); en bloc stained in Kellenberger's uranyl acetate (UA) for 2hr to overnight; dehydrated through a graded series of ethanol; and subsequently embedded in Spurr resin. Sections were cut on a Reichert Ultracut T ultramicrotome; post stained with UA and lead citrate; and observed on a Philips TEM 420 at 80kV. Images were recorded with a Soft Imaging System Megaview III digital camera; and figures were assembled in Adobe Photoshop 10.0.

Results

TDP-43 is inherently aggregation prone

To test whether TDP-43 is inherently aggregation-prone, bacterially-expressed recombinant TDP-43 was purified as a soluble protein under native conditions. Upon incubation at 25°C with agitation, TDP-43 rapidly aggregated after a lag phase of ~5-10min, as determined by an increase in turbidity (Fig. 1B) and by the amount that entered the pellet fraction after centrifugation (Fig. 1C). Several control proteins, including BSA, soybean trypsin inhibitor, creatine kinase and GFP did not aggregate under identical conditions. After 30min, no further TDP-43 aggregation occurred (Fig. 1B, C). This timeframe for TDP-43 aggregation is extended to several hours if we omit agitation during incubation (data not shown). Thus, TDP-43 is an inherently aggregation-prone protein.

It is likely that sophisticated cellular

proteostasis mechanisms (17,22), not reconstituted here, prevent such rapid TDP-43 aggregation *in vivo*. However, age-associated decline in proteostatic control in concert with environmental factors might enable TDP-43 to aggregate in disease. Regardless of the triggers of TDP-43 aggregation in disease, *in vitro* assays similar to the one we report here have been tremendously powerful tools in exploring basic mechanisms underpinning the aggregation events in Parkinson's disease (PD) and Alzheimer's disease (23-25).

Aggregates formed by pure TDP-43 did not react with the amyloid-diagnostic dyes Congo red and Thioflavin-T, in contrast to those formed by Sup35-NM, the prion domain of the yeast prion protein Sup35 (26) (Fig. 1D, E). Thus, pure TDP-43 aggregates are likely to be non-amyloid just like aggregated species of TDP-43 in ALS and FTLD-U patients (27). In ALS and FTLD-U, TDP-43 is ubiquitinated, phosphorylated, and proteolytically cleaved (4). The relative extent and contribution of these modifications to the pathogenicity of TDP-43 remains to be defined. Our *in vitro* aggregation assays will provide the foundation for future studies aimed at determining the effects of TDP-43 post-translational modification and processing on aggregation.

TDP-43's C-terminal Domain is Important for Aggregation

Next, we determined which regions of TDP-43 are critical for aggregation *in vitro*. We purified TDP-43 fragments: 1-275, which comprises the N-terminal domain, RRM1 and RRM2, and 188-414, which comprises RRM2 and the C-terminal domain (Fig. 1A). 1-275 is soluble, whereas 188-414 is the minimal fragment able to confer toxicity *and* aggregation in a yeast model of TDP-43 proteinopathies (28). Importantly, pure 1-275 did not aggregate, whereas 188-414 aggregated with similar kinetics to full-length TDP-43 (Fig. 1B). Thus, the C-terminal domain plays an important role in TDP-43 aggregation, which is striking because of the more than 25 recently reported ALS-linked TDP-43 mutations, all but one are within this domain (Fig. 2A and (12)). Furthermore, similar aggregated C-terminal fragments accumulate in ALS and FTLD-U (4). Therapeutic strategies aimed at targeting this region, which we have defined as responsible for driving aggregation, may be efficacious.

ALS-linked TDP-43 mutants form multiple aggregates in yeast

Having established that TDP-43 is inherently aggregation-prone, we next asked if ALS-linked TDP-43 mutations affect aggregation *in vivo*. We have developed a yeast TDP-43 proteinopathy model to investigate mechanisms of TDP-43 aggregation and toxicity (28). This model recapitulates several important features seen in human disease. In yeast, TDP-43 is initially localized to the nucleus but eventually forms cytoplasmic inclusions (28), mimicking the pathobiology of TDP-43 in human neurons (4). Importantly, expressing high levels of TDP-43 is toxic to yeast (28), thus possibly modeling, in a simple cell, features of neurodegeneration. We tested the effects of 7 recently reported ALS-linked mutations (6-9,11) (Fig. 2A) on TDP-43 aggregation in this system. Wild type (WT) and mutant TDP-43-YFP were expressed from a low-copy (CEN) plasmid, under control of a galactose-inducible promoter and cells were visualized by fluorescence microscopy. We confirmed that the TDP-43 proteins were expressed at comparable levels (Fig. 2B).

We compared aggregation in cells expressing WT TDP-43 to those expressing each of the 7 mutants. YFP alone was diffusely distributed between the cytoplasm and nucleus (data not shown). Strikingly, with the exception of G294A, ALS-linked mutants formed more numerous aggregates than WT TDP-43, which formed more than three cytoplasmic foci in ~4% of cells (Fig. 2C, D). Of the mutants, Q331K formed more than three cytoplasmic inclusions in >25% of cells, compared to >10% of cells for the other TDP-43 mutants (Fig. 2C, D). GFP-tagged protein fusions can occasionally produce artifactual aggregation (29). Hence, we confirmed these results by performing immunocytochemistry, with a TDP-43-specific antibody, on cells expressing untagged WT and a representative selection of mutant TDP-43 constructs (Fig. 2E). Untagged Q331K and M337V typically formed more discrete aggregates per cell than WT or G294A (Fig. 2E).

To confirm that TDP-43 foci visualized by microscopy represented insoluble aggregates, we performed a sedimentation analysis (19). As

a negative control, we used YFP expressing cells. YFP was entirely soluble (Fig. 2F). As positive controls, we used 25Q and 103Q containing fragments from exon 1 of huntingtin. In our yeast sedimentation assay, these proteins also partitioned between soluble and insoluble, with 25Q being mostly soluble and 103Q being mostly insoluble (Fig. 2F). WT and mutant TDP-43 partitioned between soluble and insoluble fractions (Fig. 2F). Thus, TDP-43 forms insoluble aggregates in yeast. After 6h of expression similar quantities of TDP-43 formed insoluble aggregates in cells expressing WT, G294A, M337V and Q331K TDP-43 (Fig. 2F). However, our fluorescence microscopy data suggest that this total amount of insoluble protein appears to be distributed among more numerous discrete aggregates for M337V and Q331K (Fig. 2C, D) and is concentrated in fewer foci for G294A and WT (Fig. 2C, D). It may be that Q331K (and M337V) aggregates more rapidly than WT TDP-43, but that after 6h of expression both have reached a saturating level of aggregation. Therefore, we focused on Q331K, which formed the most foci of the mutants tested (Fig. 2C) and performed sedimentation analysis at earlier time-points. At 4h, there was a greater relative amount of Q331K in the pellet fraction than WT TDP-43 (Fig. 2G), consistent with this mutation accelerating aggregation. However, the sedimentation assay may not be sensitive enough to detect subtle differences in TDP-43 aggregation between WT and the other ALS-linked mutants in yeast, like those we observe by fluorescence microscopy. Therefore, to resolve these issues, additional *in vitro* assays are required to define quantitatively the contribution of ALS-linked mutations to TDP-43's biochemical properties (i.e. aggregation; for example, see Fig. 5 below).

Next, we used fluorescence microscopy to compare the aggregation of WT TDP-43 and one of the mutants (Q331K) over time. Even at very early time points (e.g. 2 hours), we observed many more aggregates per cell with Q331K TDP-43 than with WT (Fig. 2H). Thus, ALS-linked mutations in TDP-43 can increase the number of discrete aggregates in the yeast cytoplasm.

Finally, we used electron microscopy to visualize aggregates formed by TDP-43 *in vivo*. In the yeast cytoplasm, Q331K TDP-43 formed discrete aggregated foci of ~0.2μm in diameter (Fig. 3) that were not observed in control cells (data not shown). TDP-43 aggregates formed in yeast cells possessed a granular morphology (Fig. 3) similar to TDP-43 aggregates in ALS and FTLD-U (30-32) and to those formed *in vitro* using pure protein (see below).

ALS-linked TDP-43 mutants are more toxic in yeast

Next, we investigated the effects of ALS-linked TDP-43 mutations on toxicity. In yeast, expression of WT TDP-43 at high levels (2μ plasmid) is extremely toxic (28). Since we wanted to compare toxicity between WT and mutant TDP-43, we used a low-copy CEN plasmid to express TDP-43-YFP at a level that was only slightly toxic. We performed spotting assays to compare growth defects elicited by WT and by ALS-linked TDP-43 mutants (Fig. 4). The 6 ALS-linked mutants that formed more discrete aggregates than WT (Fig. 2) were also more toxic (Fig. 4B, C). The Q331K mutant that consistently formed the most numerous aggregated foci in yeast (Fig. 2D) was considerably more toxic than WT or the other mutants (Fig. 4B, C), despite being expressed at the same level as the other proteins (Fig. 2B). G294A was similar to WT in both number of aggregated foci per cell (Fig. 2D) and toxicity (Fig. 4B). We obtained similar results using either YFP-tagged (Fig. 4B) or untagged constructs (Fig. 4C).

The growth defect elicited by TDP-43 in our spotting assays could reflect either cell death or simply a growth arrest. To distinguish between these two possibilities, we performed survivorship assays, in which we determined the ability of cells to form a colony upon cessation of TDP-43 expression. When we used the high-copy 2 micron plasmid to express WT TDP-43 and a subset of the mutants, fewer than 10% of cells were able to form colonies following 12 hours of expression and by 24 hours fewer than 2% were still alive (Fig. 4D). We were able to detect differences in survivorship between WT and the mutants by using the low copy CEN plasmid. While 100% of cells containing an empty vector were able to form a colony, following 12 hours of galactose induction, only approximately 30% of cells that had expressed WT, M337V, or G294A TDP-43 were able to form a colony and only approximately 10% of

Q331K-expressing cells formed colonies. This survivorship assay is not as sensitive as the spotting assays. Thus, with the survivorship assay, we were unable to detect the subtle differences in growth between WT and M337V that we saw by spotting (Fig. 4B, C).

To further confirm cell death as opposed to simple growth arrest, we employed propidium iodide (PI), a fluorescent dye that binds DNA. PI is membrane impermeant and is generally excluded from viable cells. TDP-43-expressing cells stained positive for PI (Fig. 4E), which indicates a loss of cell viability. Thus, in yeast TDP-43 aggregation leads to cell death and not simply a growth arrest. Moreover, several ALS-linked TDP-43 mutations can increase the number of TDP-43 aggregates and enhance toxicity.

ALS-linked TDP-43 Mutations Can Accelerate TDP-43 Aggregation

We then used pure proteins to determine whether three of the ALS-linked TDP-43 mutations affected the aggregation process directly. We selected Q331K and M337V, which formed more aggregated foci than WT, and G294A, which formed similar numbers of aggregated foci to WT in yeast (Fig. 2D). The formation of multiple aggregated foci by Q331K and M337V *in vivo* might reflect more rapid nucleation of aggregation, which can result in more numerous aggregates (33). Consistent with our *in vivo* data, the Q331K and M337V mutants aggregated much more rapidly than WT (Fig. 5A, B), whereas G294A did not accelerate TDP-43 aggregation and resembled WT (Fig. 5A, B). Specifically, the lag phase of aggregation was greatly reduced for both Q331K and M337V compared to WT and G294A (Fig. 5A, B). Q331K aggregated even more rapidly than M337V (Fig. 5A, B), consistent with Q331K forming more numerous aggregates in yeast. Moreover, more Q331K protein was insoluble than WT protein after 4h of expression in yeast, consistent with more rapid assembly kinetics (Fig. 2G). These data suggest that the Q331K and M337V mutations likely alter the TDP-43 folding landscape such that aggregation is more energetically favorable. However, even though Q331K and M337V aggregated more rapidly than WT or G294A *in vitro*, the final amount of aggregated protein after 30-60min was similar for all TDP-43 variants (Fig. 5A, B). Similarly, after six hours of expression *in vivo* these TDP-43 variants formed approximately equal quantities of insoluble protein (Fig. 2F).

Pure TDP-43 Aggregates Resemble TDP-43 Aggregates in Degenerating Neurons in ALS and FTLD-U

Electron microscopy (EM) revealed that WT TDP-43 and G294A rapidly formed small oligomeric complexes after 5min (Fig. 6A, examples denoted by arrowheads), which would sometimes adopt a pore-like conformation (Fig. 6B), strikingly akin to the pathological oligomers formed by Aβ42 and α-synuclein (34). To confirm that these conformers were TDP-43 oligomers, we performed size exclusion chromatography. Consistent with previous reports (35), WT TDP-43 eluted from a Superdex-200 gel filtration column as predominantly dimeric and monomeric species (Fig. 6C). However, a small fraction eluted as higher order oligomers (Fig. 6C). Inspection of the pooled oligomeric fraction by EM revealed oligomeric profiles similar to those observed at early times during aggregation reactions (Fig. 6D).

Incubation of TDP-43 for longer times (15-60min) with agitation induced the formation of short filament-like structures (Fig. 6A, examples denoted by small arrows), which clustered together with oligomers to form large masses by 30-60min (Fig. 6A). EM of supernatant and pellet fractions demonstrated that some small oligomers remain in the supernatant fraction, whereas clusters of oligomers and larger species enter the pellet fraction (Fig. 6E).

G294A formed aggregates that tended to be more amorphous and less well resolved than WT (Fig. 6A). The large masses of oligomeric forms populated by pure TDP-43 are remarkably similar to those observed in ALS and FTLD-U patients, which can displace cytoplasmic organelles (30-32). For example, WT TDP-43 aggregates in Fig. 6A (30min or 60min) appear morphologically similar to the TDP-43 inclusions in the neurons of ALS patients in Fig. 3c-f in (31) or in the neurons and glial cells of ALS patients in Fig. 2 of (32).

M337V aggregated in a similar manner (Fig. 6A, B), except that oligomers and filament-like structures clustered together much

earlier, and proceeded to form larger masses than WT or G294A (Fig. 6A). By contrast, Q331K passed through similar oligomeric forms as WT, G294A and M337V (Fig. 6A, B), but eventually accessed morphologically distinct aggregated forms, with a thread- or skein-like appearance (Fig. 6A, examples denoted by large arrows). Similar thread-like structures that immunolabel for TDP-43 are observed regularly in the degenerating neurons of ALS and FTLD-U patients (30-32). For example, compare Q331K TDP-43 aggregates formed with pure protein in Fig. 7A to those in neurons of FTLD-U patients in Fig. 2b, d of (30) or in neurons of ALS patients in Fig. 6c, d of (30). The pure Q331K structures differ subtly from those observed in patients, in that they are slightly less regular and are typically more filamentous and not granulo-filamentous. Nonetheless, their overall similarity is striking.

Although less abundant, similar threadlike structures were also formed by WT TDP-43 (Fig. 7A), as well as G294A and M337V (data not shown). Typically, these forms are shorter and more ragged than those observed in ALS or FTLD-U patients. However, after extended incubations, occasionally longer, smoother granulo-filamentous WT TDP-43 aggregates were observed (Fig. 7B). These structures are strikingly reminiscent of aggregated species populated by TDP-43 in the degenerating neurons of ALS and FTLD-U patients (30-32).

Discussion

In sum, we have faithfully reconstructed several aspects of the pathological TDP-43 aggregation process using solely pure TDP-43. Our data establish that pure TDP-43 forms aggregated species *in vitro* that are remarkably similar to the TDP-43 aggregates in FTLD-U and ALS patients. Further, we show that pathogenic mutations in the TDP-43 gene can accelerate aggregation *in vitro* and elicit the formation of more numerous aggregates *in vivo*. Thus, it seems likely that TDP-43 is a key aggregated protein in ALS and FTLD-U, just as α-synuclein is in Parkinson's disease (PD) and tau and amyloid-β are in Alzheimer's disease (36).

6 of 7 ALS-linked TDP-43 mutants that we tested, especially Q331K, induced the formation of multiple TDP-43 aggregates per cell. Although, at 4h we observed an increase in aggregation of Q331K compared to WT (Fig. 2G), by sedimentation analysis we could not detect differences in the total amount of insoluble TDP-43 between WT and the mutants expressed for 6h in yeast (Fig. 2F). This may simply reflect the endpoint of aggregation *in vivo*, just as similar amounts of TDP-43 eventually form aggregates *in vitro*, regardless of the TDP-43 variant. Furthermore, the sedimentation assay might not be sensitive enough to allow us to discern the significant differences in aggregation patterns observed by microscopy. The 25Q versus 103Q huntingtin constructs clearly showed a difference in insolubility in the sedimentation assay. However, huntingtin fragments with polyglutamine tracts of ~25Q do not typically aggregate *in vitro* or *in vivo* (37,38). Thus, a large difference was expected. Moreover, our TDP-43 mutants only differ from WT by a single residue.

Rather, we suggest that the ALS-linked mutations might affect the morphology and/or localization of the aggregates *in vivo* rather than the total amount of insoluble TDP-43 (as detected by sedimentation assay). For example, with WT TDP-43, we frequently observe one large juxtanuclear focus (Fig. 2C), reminiscent of the recently described JUNQ ('juxtanuclear quality control') compartment where misfolded proteins accumulate (19). The observation that ALS-linked TDP-43 mutants tend to form multiple foci *in vivo* (Fig. 2C) might be attributable to the accelerated kinetics of aggregation, which we observe *in vitro* (Fig. 5), enabling them to escape this quality control mechanism and thus be more toxic than WT. Nevertheless, the two mutants that consistently formed multiple aggregated foci in yeast, Q331K and M337V, also aggregated more rapidly *in vitro*, in our pure protein assays. Thus, a single amino acid change is sufficient to accelerate TDP-43 misfolding, supporting the notion that some ALS-linked mutations can cause disease by a toxic 'gain-of-function mechanism' at the protein level. The mutations that accelerate spontaneous aggregation *in vitro* and form multiple aggregated foci *in vivo* are also more toxic (Fig. 4), suggesting that a subset of ALS-linked TDP-43 mutations may cause disease by accelerating TDP-43 aggregation and contingent toxicity. ALS-linked TDP-43

mutants with accelerated aggregation and toxicity are reminiscent of PD-linked α−synuclein mutants (A30P, A53T, E46K) that oligomerize or fibrillize more rapidly and are connected with early-onset PD (23,24,39).

So far, it does not appear that TDP-43 mutations are a common cause of ALS (40). Thus, there are likely other pathogenic mechanisms, some which converge on TDP-43 and others that do not. Nonetheless, it is apparent that TDP-43 pathology is very commonly associated with sporadic and non-SOD1 familial ALS (41). Thus, studying TDP-43 aggregation and toxicity *in vitro* and *in vivo*, as reported here, will likely help to elucidate the role of TDP-43 in pathogenesis. Furthermore, given TDP-43's dose-dependent toxicity (28) and aggregation-prone nature, increased TDP-43 levels might accelerate ALS just as increased wild type α−synuclein levels accelerate PD (42). Therefore, TDP-43 copy number, promoter and regulatory regions should also be analyzed in the context of ALS, FTLD-U and other TDP-43 proteinopathies.

Why is Q331K considerably more toxic than the other mutants we tested in our yeast model? We note that pure Q331K more readily accessed thread-like aggregated forms, and grossly similar inclusions are consistently found in motor neurons undergoing neuronophagia, the final step in motor neuron death in sporadic ALS (43). Thus far, there has been one reported patient with this mutation (7), and it has not been found in thousands of control samples. Future studies using animal models (e.g. mouse, *Drosophila*, *C. elegans*, and zebrafish) will provide additional insights into the effects of WT versus mutant TDP-43 in neurodegeneration.

Other TDP-43 mutations, e.g. M337V, have been identified in multiple individuals and segregate with disease in familial ALS (7). Another mutation, Q343R, is also associated with familial ALS and patients present with more widespread TDP-43 pathology than most non-mutant TDP-43 cases (11). Remarkably, Q343R also aggregates more extensively and is more toxic in our yeast model (Figs. 2, 4). However, because exhaustive genetic studies of TDP-43 in ALS and FTLD-U have not yet been performed, it is probably too soon to judge the potential pathogenicity of every single TDP-43 mutation that has been found in patients. One recent report found that TDP-43 pathology in a patient harboring the G294A mutation was similar to that of patients without this lesion (44). Interestingly, G294A behaved like WT TDP-43 in our yeast and pure protein assays, further corroborating these approaches.

Our yeast model will facilitate assessment of the effects of newly identified mutations on aggregation and toxicity. To our knowledge, there are no available tissue culture models that recapitulate both TDP-43 aggregation and toxicity. Given the previous success defining disease mechanisms and mammalian genetic suppressors of PD using a yeast synucleinopathy model (18,45,46), genome-wide approaches using the yeast TDP-43 model are likely to provide insight into disease mechanism, identify potential biomarkers, and suggest avenues for therapeutic strategies. Finally, the pure TDP-43 aggregation assay described here will empower us to identify small molecules and cellular factors able to inhibit or even reverse TDP-43 aggregation.

References

1 Ayala, Y. M., Pantano, S., D'Ambrogio, A., Buratti, E., Brindisi, A., Marchetti, C., Romano, M., and Baralle, F. E. (2005) *J Mol Biol* **348**, 575-588

2 Ayala, Y. M., Misteli, T., and Baralle, F. E. (2008) *Proc Natl Acad Sci U S A* **105**, 3785-3789

3 Buratti, E., and Baralle, F. E. (2001) *J Biol Chem* **276**, 36337-36343

4 Neumann, M., Sampathu, D. M., Kwong, L. K., Truax, A. C., Micsenyi, M. C., Chou, T. T., Bruce, J., Schuck, T., Grossman, M., Clark, C. M., McCluskey, L. F., Miller, B. L., Masliah, E., Mackenzie, I. R., Feldman, H., Feiden, W., Kretzschmar, H. A., Trojanowski, J. Q., and Lee, V. M. (2006) *Science* **314**, 130-133

5 Forman, M. S., Trojanowski, J. Q., and Lee, V. M. (2007) *Curr Opin Neurobiol*

6 Kabashi, E., Valdmanis, P. N., Dion, P., Spiegelman, D., McConkey, B. J., Vande Velde, C., Bouchard, J. P., Lacomblez, L., Pochigaeva, K., Salachas, F., Pradat, P. F., Camu, W., Meininger, V., Dupre, N., and Rouleau, G. A. (2008) *Nat Genet* **40**, 572-574
7 Sreedharan, J., Blair, I. P., Tripathi, V. B., Hu, X., Vance, C., Rogelj, B., Ackerley, S., Durnall, J. C., Williams, K. L., Buratti, E., Baralle, F., de Belleroche, J., Mitchell, J. D., Leigh, P. N., Al-Chalabi, A., Miller, C. C., Nicholson, G., and Shaw, C. E. (2008) *Science* **319**, 1668-1672
8 Van Deerlin, V. M., Leverenz, J. B., Bekris, L. M., Bird, T. D., Yuan, W., Elman, L. B., Clay, D., Wood, E. M., Chen-Plotkin, A. S., Martinez-Lage, M., Steinbart, E., McCluskey, L., Grossman, M., Neumann, M., Wu, I. L., Yang, W. S., Kalb, R., Galasko, D. R., Montine, T. J., Trojanowski, J. Q., Lee, V. M., Schellenberg, G. D., and Yu, C. E. (2008) *Lancet Neurol* **7**, 409-416
9 Rutherford, N. J., Zhang, Y. J., Baker, M., Gass, J. M., Finch, N. A., Xu, Y. F., Stewart, H., Kelley, B. J., Kuntz, K., Crook, R. J., Sreedharan, J., Vance, C., Sorenson, E., Lippa, C., Bigio, E. H., Geschwind, D. H., Knopman, D. S., Mitsumoto, H., Petersen, R. C., Cashman, N. R., Hutton, M., Shaw, C. E., Boylan, K. B., Boeve, B., Graff-Radford, N. R., Wszolek, Z. K., Caselli, R. J., Dickson, D. W., Mackenzie, I. R., Petrucelli, L., and Rademakers, R. (2008) *PLoS Genet* **4**, e1000193
10 Gitcho, M. A., Baloh, R. H., Chakraverty, S., Mayo, K., Norton, J. B., Levitch, D., Hatanpaa, K. J., White, C. L., 3rd, Bigio, E. H., Caselli, R., Baker, M., Al-Lozi, M. T., Morris, J. C., Pestronk, A., Rademakers, R., Goate, A. M., and Cairns, N. J. (2008) *Ann Neurol*. 63, 535-538
11 Yokoseki, A., Shiga, A., Tan, C. F., Tagawa, A., Kaneko, H., Koyama, A., Eguchi, H., Tsujino, A., Ikeuchi, T., Kakita, A., Okamoto, K., Nishizawa, M., Takahashi, H., and Onodera, O. (2008) *Ann Neurol* **63**, 538-542
12 Banks, G. T., Kuta, A., Isaacs, A. M., and Fisher, E. M. (2008) *Mamm Genome* **19**, 299-305
13 Rothstein, J. D. (2007) *Ann Neurol* **61**, 382-384
14 Arai, T., Hasegawa, M., Akiyama, H., Ikeda, K., Nonaka, T., Mori, H., Mann, D., Tsuchiya, K., Yoshida, M., Hashizume, Y., and Oda, T. (2006) *Biochem Biophys Res Commun* **351**, 602-611
15 Sanelli, T., Xiao, S., Horne, P., Bilbao, J., Zinman, L., and Robertson, J. (2007) *J Neuropathol Exp Neurol* **66**, 1147-1153
16 Xiao, S., Tjostheim, S., Sanelli, T., McLean, J. R., Horne, P., Fan, Y., Ravits, J., Strong, M. J., and Robertson, J. (2008) *J Neurosci* **28**, 1833-1840
17 Balch, W. E., Morimoto, R. I., Dillin, A., and Kelly, J. W. (2008) *Science* **319**, 916-919
18 Cooper, A. A., Gitler, A. D., Cashikar, A., Haynes, C. M., Hill, K. J., Bhullar, B., Liu, K., Xu, K., Strathearn, K. E., Liu, F., Cao, S., Caldwell, K. A., Caldwell, G. A., Marsischky, G., Kolodner, R. D., Labaer, J., Rochet, J. C., Bonini, N. M., and Lindquist, S. (2006) *Science* **313**, 324-328
19 Kaganovich, D., Kopito, R., and Frydman, J. (2008) *Nature* **454**, 1088-1095
20 Chernoff, Y. O., Uptain, S. M., and Lindquist, S. L. (2002) *Methods Enzymol* **351**, 499-538
21 Rieder, S. E., Banta, L. M., Kohrer, K., McCaffery, J. M., and Emr, S. D. (1996) *Mol Biol Cell* **7**, 985-999
22 Morimoto, R. I. (2008) *Genes Dev* **22**, 1427-1438
23 Conway, K. A., Harper, J. D., and Lansbury, P. T. (1998) *Nat Med* **4**, 1318-1320
24 Conway, K. A., Lee, S. J., Rochet, J. C., Ding, T. T., Williamson, R. E., and Lansbury, P. T., Jr. (2000) *Proc Natl Acad Sci U S A* **97**, 571-576
25 Lashuel, H. A., Hartley, D. M., Petre, B. M., Wall, J. S., Simon, M. N., Walz, T., and Lansbury, P. T., Jr. (2003) *J Mol Biol* **332**, 795-808
26 Shorter, J., and Lindquist, S. (2005) *Nat Rev Genet* **6**, 435-450
27 Kwong, L. K., Uryu, K., Trojanowski, J. Q., and Lee, V. M. (2008) *Neurosignals* **16**, 41-51
28 Johnson, B. S., McCaffery, J. M., Lindquist, S., and Gitler, A. D. (2008) *Proc Natl Acad Sci U S A* **105**, 6439-6444
29 McLean, P. J., Kawamata, H., and Hyman, B. T. (2001) *Neuroscience* **104**, 901-912
30 Lin, W. L., and Dickson, D. W. (2008) *Acta Neuropathol* **116**, 205-213
31 Mori, F., Tanji, K., Zhang, H. X., Nishihira, Y., Tan, C. F., Takahashi, H., and Wakabayashi, K. (2008) *Acta Neuropathol* **116**, 193-203
32 Nishihira, Y., Tan, C. F., Onodera, O., Toyoshima, Y., Yamada, M., Morita, T., Nishizawa, M., Kakita, A., and Takahashi, H. (2008) *Acta Neuropathol* **116**, 169-182
33 Scheibel, T., Parthasarathy, R., Sawicki, G., Lin, X. M., Jaeger, H., and Lindquist, S. L. (2003) Proc Natl

Acad Sci U S A 100, 4527-4532
34 Lashuel, H. A., Hartley, D., Petre, B. M., Walz, T., and Lansbury, P. T., Jr. (2002) *Nature* **418**, 291
35 Kuo, P. H., Doudeva, L. G., Wang, Y. T., Shen, C. K., and Yuan, H. S. (2009) *Nucleic Acids Res* **37**(6):1799-808
36 Skovronsky, D. M., Lee, V. M., and Trojanowski, J. Q. (2006) *Annu Rev Pathol* **1**, 151-170
37 Scherzinger, E., Lurz, R., Turmaine, M., Mangiarini, L., Hollenbach, B., Hasenbank, R., Bates, G. P., Davies, S. W., Lehrach, H., and Wanker, E. E. (1997) *Cell* **90**, 549-558
38 Krobitsch, S., and Lindquist, S. (2000) *Proc Natl Acad Sci U S A* **97**, 1589-1594
39 Choi, W., Zibaee, S., Jakes, R., Serpell, L. C., Davletov, B., Crowther, R. A., and Goedert, M. (2004) *FEBS Lett* **576**, 363-368
40 Daoud, H., Valdmanis, P. N., Kabashi, E., Dion, P., Dupre, N., Camu, W., Meininger, V., and Rouleau, G. A. (2008) *J Med Genet* 46, 112-114
41 Mackenzie, I. R., Bigio, E. H., Ince, P. G., Geser, F., Neumann, M., Cairns, N. J., Kwong, L. K., Forman, M. S., Ravits, J., Stewart, H., Eisen, A., McClusky, L., Kretzschmar, H. A., Monoranu, C. M., Highley, J. R., Kirby, J., Siddique, T., Shaw, P. J., Lee, V. M., and Trojanowski, J. Q. (2007) *Ann Neurol* **61**, 427-434
42 Singleton, A. B., Farrer, M., Johnson, J., Singleton, A., Hague, S., Kachergus, J., Hulihan, M., Peuralinna, T., Dutra, A., Nussbaum, R., Lincoln, S., Crawley, A., Hanson, M., Maraganore, D., Adler, C., Cookson, M. R., Muenter, M., Baptista, M., Miller, D., Blancato, J., Hardy, J., and Gwinn-Hardy, K. (2003) *Science* **302**, 841
43 Pamphlett, R., and Kum Jew, S. (2008) *Acta Neuropathol* **116**, 221-222
44 Pamphlett, R., Luquin, N., McLean, C., Jew, S. K., and Adams, L. (2008) *Neuropathol Appl Neurobiol* 35, 222-225
45 Gitler, A. D., Chesi, A., Geddie, M. L., Strathearn, K. E., Hamamichi, S., Hill, K. J., Caldwell, K. A., Caldwell, G. A., Cooper, A. A., Rochet, J. C., and Lindquist, S. (2009) *Nat Genet* **41**, 308-315
46 Yeger-Lotem, E., Riva, L., Su, L. J., Gitler, A. D., Cashikar, A. G., King, O. D., Auluck, P. K., Geddie, M. L., Valastyan, J. S., Karger, D. R., Lindquist, S., and Fraenkel, E. (2009) *Nat Genet* **41**, 316-323

Acknowledgments
We thank Greg Van Duyne for pGV13, Mark Lemmon, Jon Epstein and Nancy Bonini for comments on the manuscript. This work was supported in part by a Pilot grant from the University of Pennsylvania Institute on Aging (A.D.G.) and by NIH Director's New Innovator Awards 1DP2OD004417-01 (A.D.G.) and 1DP2OD002177-01 (J.S.). A.D.G. is a Pew Scholar in the Biomedical Sciences, supported by The Pew Charitable Trusts.

Figure legends

Figure 1. Aggregation of TDP-43 and TDP-43 fragments *in vitro*. (A) A diagram of the domain structure of TDP-43 indicating both RNA recognition motifs (RRM1 and RRM2) and the glycine-rich C-terminal domain. **(B)** TDP-43 or the indicated TDP-43 fragment (1-275 or 188-414) (3μM) were incubated at 25°C with agitation for 0-120min. The extent of aggregation was determined by turbidity. Values represent means±SD (n=3). **(C)** Aggregation of WT TDP-43 as in **(B)** assessed by sedimentation analysis. Values represent means±SD (n=3). **(D)** His-TDP-43 or Sup35-NM (5μM) were incubated for either 0min (soluble protein) or 2h (aggregated protein) at 25°C with agitation. Reactions were then processed for Congo Red Binding. Values represent means±SD (n=3). **(E)** TDP-43 or Sup35-NM (5μM) were incubated for either 0min (soluble protein) or 2h (aggregated protein) at 25°C with agitation. Reactions were then processed for Thioflavin-T fluorescence. Values represent means±SD (n=3).

Figure 2. Aggregation of TDP-43 and ALS-linked mutants *in vivo*. (A) Schematic indicating disease-associated TDP-43 mutations. Color code of mutations indicates aggregation compared to WT (red = considerably more aggregates than WT; green = more aggregates than WT; black = as many aggregates as

WT). **(B)** YFP alone, WT and mutant TDP-43-YFP expression levels were determined by immunoblotting with an anti-GFP antibody. Phosphoglycerate kinase 1 (Pgk1) was used as a loading control. **(C)** Representative fluorescent microscopy images of DAPI-stained (blue to denote the position of the nucleus) WT or mutant TDP-43-YFP (green). **(D)** The effect of TDP-43 mutations on aggregation *in vivo* was quantified by counting the number of cells containing > 3 foci. Values represent means ± SEM (n≥3, at least 200 cells per sample). Cells expressing YFP alone did not contain foci (data not shown). **(E)** Untagged TDP-43 also forms aggregates in yeast cells. Immunocytochemistry with an anti-TDP-43 antibody was used to visualize TDP-43 expression. Arrows point to cytoplasmic TDP-43 inclusions. Cells transformed with an empty vector were used as a control for antibody specificity. **(F)** Sedimentation assay to demonstrate TDP-43 forms insoluble aggregates in yeast cells. Yeast cells expressing YFP, htt25QCFP, htt103Q-CFP, or WT and mutant TDP-43-YFP for 6h were lysed and processed for sedimentation assay as in (19). Soluble and insoluble fractions were separated by centrifugation. 20% of the pellet fraction and 10% of soluble and total fractions were resolved by SDS-PAGE followed by immunoblotting with anti-GFP antibody. Whereas YFP was completely soluble, WT and TDP-43 partitioned into soluble and insoluble fractions, similar to the aggregation-prone fragments of the huntingtin protein (htt25Q (mostly soluble) or htt103Q (mostly insoluble)). Arrow indicates top of gel. **(G)** Sedimentation assay performed as in **F** except that WT and Q331K TDP-43 constructs were induced for 4h. At this time-point, a greater relative amount of Q331K is present in the insoluble pellet fraction than WT TDP-43. T, total; S, soluble; P, pellet. Representative image from three separate experiments is shown. **(H)** Time-course analysis of WT and Q331K TDP-43 aggregation demonstrates Q331K forms more discrete aggregates than WT at early time points.

Figure 3. EM of TDP-43 aggregates in yeast. (A-C). Low magnification TEM shows an example of a granular aggregate in yeast cells expressing the Q331K TDP-43 mutant (boxed region, **(A)**; high magnification +25° tilt view of boxed region in **A**. **(B)**, and additional high magnification view of TDP-43 aggregate **(C)**. m=mitochondria; V=vacuole; arrowheads delineate TDP-43 aggregate; bars=0.25μm.

Figure 4. The effect of ALS-linked TDP-43 mutations on toxicity. (A) Schematic indicating disease-associated TDP-43 mutations shown above. Color code of mutations indicates toxicity compared to WT (red = considerably more toxic than WT; green = slightly more toxic than WT; black = as toxic as WT). **(B)** Spotting assay to compare the toxicity of WT and mutant TDP-43. Serial dilutions of yeast cells transformed with galactose-inducible YFP, WT or mutant TDP-43-YFP constructs. Transformants were spotted on glucose (non-inducing) or galactose (inducing) containing agar plates, and growth assessed after 48 to 72 hours. **(C)** Spotting assay to compare the toxicity of WT and mutant TDP-43. Serial dilutions of yeast cells transformed with galactose-inducible untagged WT or mutant TDP-43 constructs. Transformants were spotted on glucose (non-inducing) or galactose (inducing) containing agar plates, and growth assessed after 48 to 72 hours. **(D)** Survivorship curve during TDP-43 induction, using the high copy 2 micron vector. After induction of empty vector, TDP-43 WT, G294A, Q331K, or M337V, survivorship was determined at the indicated time-points by harvesting cells at OD_{600nm} = 1, diluting 1:1000 and plating 300 μl of these cells on to synthetic media containing 2% glucose (represses TDP-43 expression). Plates were incubated at 30°C and colony forming units were determined after 2 days. **(E)** TDP-43 expression causes cell death. TDP-43 expression was induced for 6 hours and cells were stained with propidium iodide (PI) to assess viability. WT and mutant TDP-43-expressing cells were positive for PI staining (indicating cell death), whereas empty-vector containing cells were negative for PI staining (indicating viability).

Figure 5. Q331K and M337V accelerate spontaneous TDP-43 aggregation. (A, B) TDP-43 or the indicated ALS-linked TDP-43 mutant (Q331K, M337V or G294A) (3μM) were incubated at 25°C with agitation for 0-60min. The extent of aggregation was determined by turbidity **(A)** or sedimentation analysis **(B)**. Values represent means±SD (n=3). Inset **(A)** the equal input of TDP-43 proteins is shown on a Coomassie stained gel.

Figure 6. Pure TDP-43 and ALS-linked mutant aggregates resemble TDP-43 aggregates in

degenerating neurons of ALS patients. (A) TDP-43 or the indicated ALS-linked TDP-43 mutant (Q331K, M337V or G294A) (3μM) were incubated at 25°C with agitation for 0-60min. At various times, reactions were processed for EM. Arrowheads denote small oligomers, small arrows denote filament-like structures and large arrows denote thread-like structures. Bar, 0.5μm. **(B)** Gallery of TDP-43 and ALS-linked TDP-43 mutant oligomers formed after 5min. Bar, 50nm. **(C)** TDP-43 was incubated at 25°C with agitation for 5min and processed for Superdex-200 size exclusion chromatography. TDP-43 eluted as a predominantly dimeric and monomeric species, but a small fraction eluted as oligomeric species. Arrows at the top indicate elution volumes of the molecular weight standards. **(D)** EM of oligomeric pool eluted from the Superdex-200 column. Bar, 50nm. **(E)** TDP-43 (3μM) was incubated at 25°C with agitation for 30min. Supernatant and pellet fractions were separated and processed for EM. Bar, 100nm.

Figure 7. Thread-like aggregates formed by TDP-43.
(A) Gallery of thread-like aggregates of TDP-43 and Q331K formed after 60min of agitation at 25°C. Bar, 100nm. **(B)** Longer and more regular granulo-filamentous forms populated by WT TDP-43 after 2h of agitation at 25°C. Bar, 100nm.

Figure 1

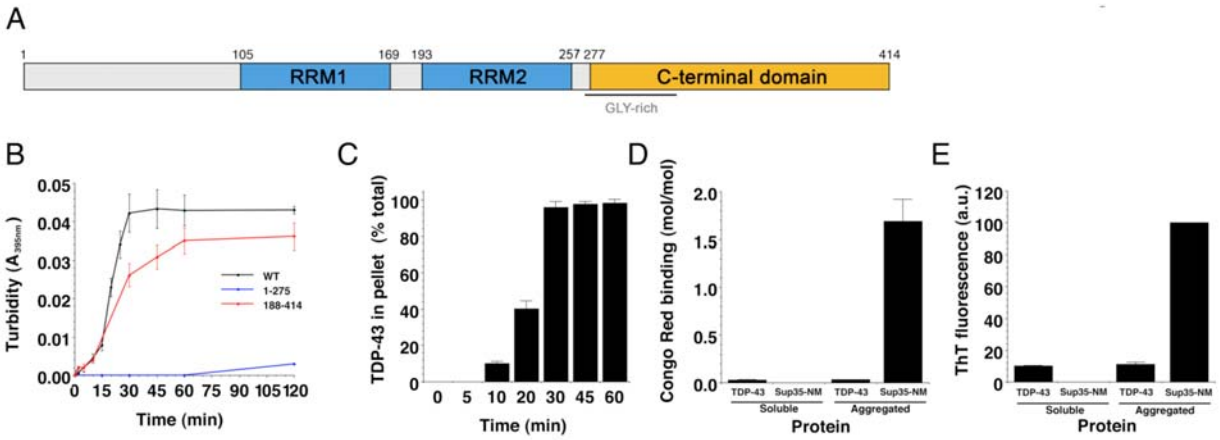

Figure 2

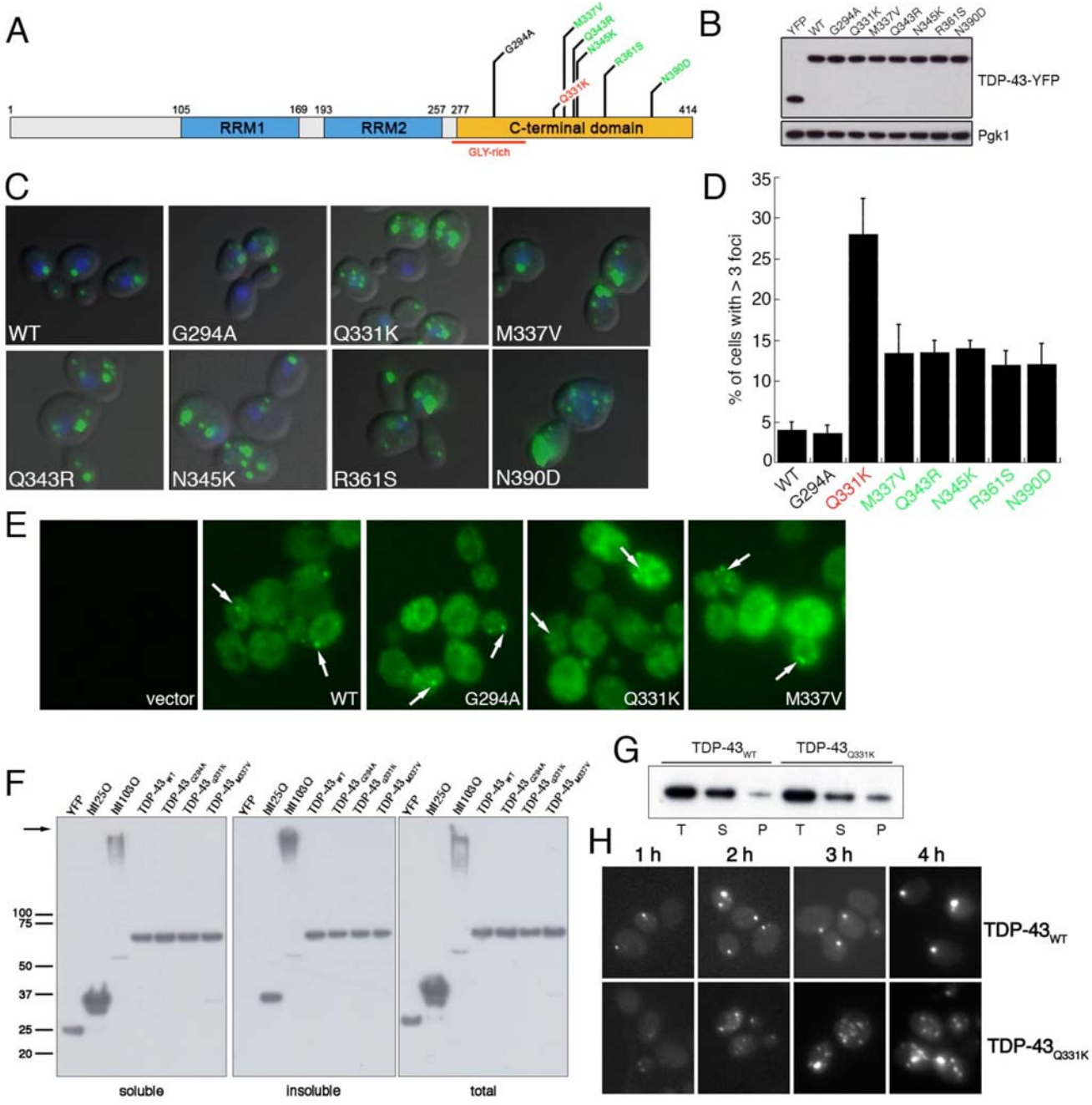

Figure 3

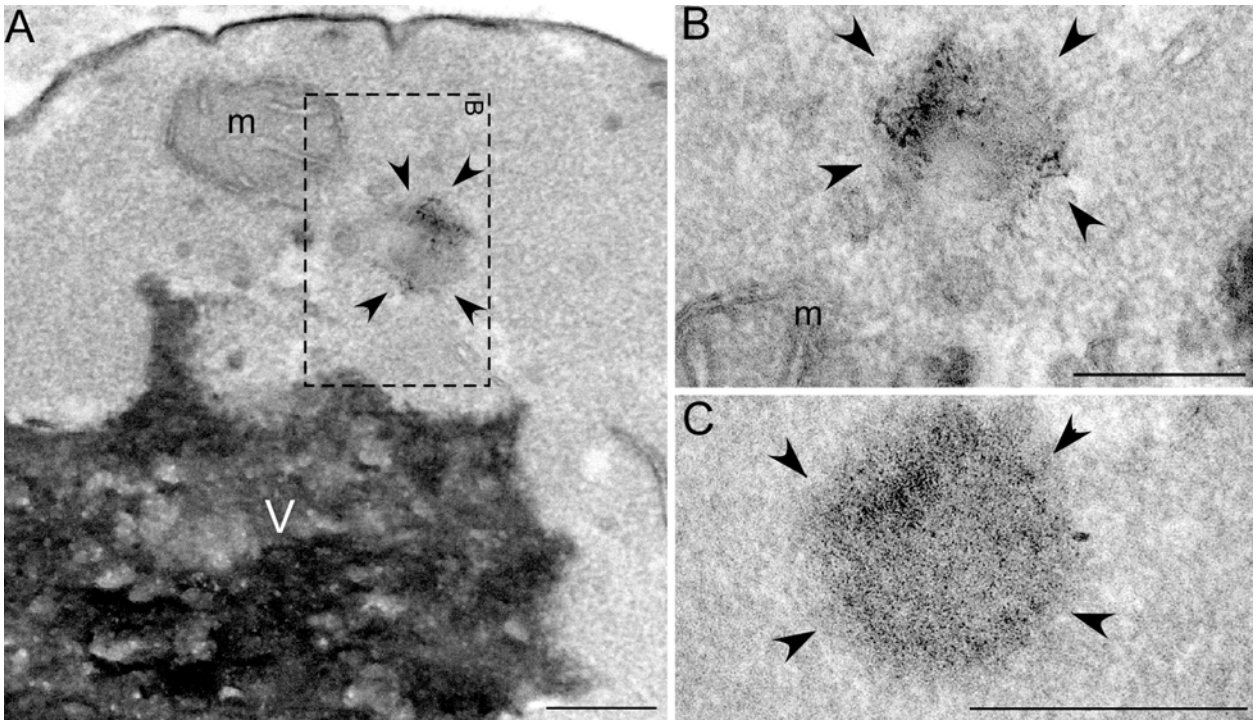

Figure 4

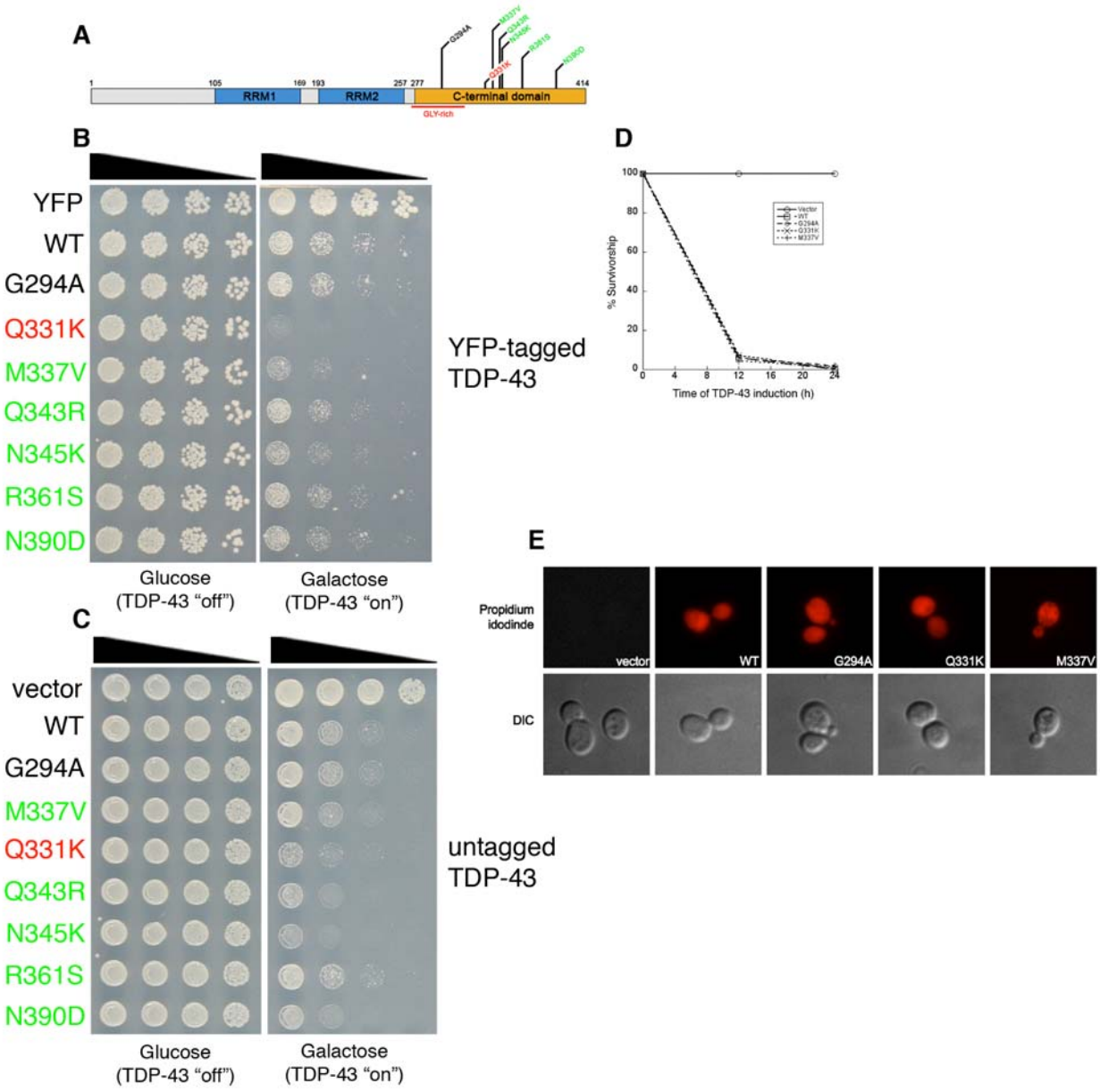

Figure 5

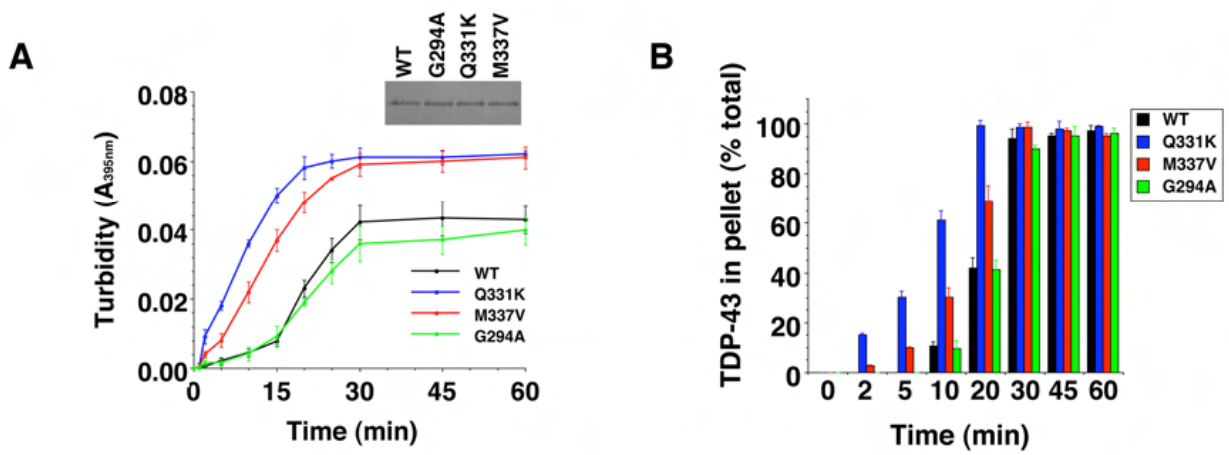

Figure 6

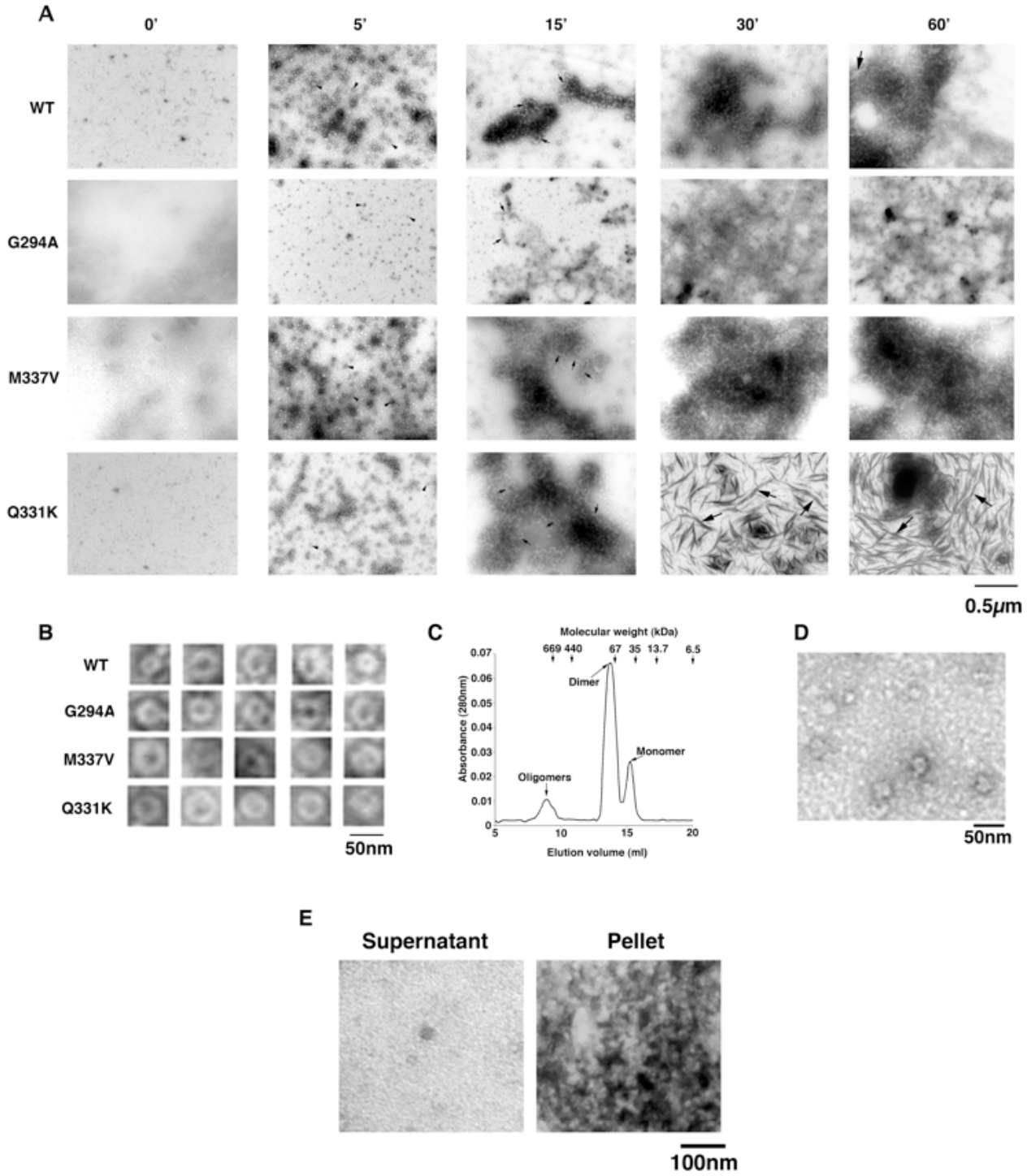

Figure 7